

# Adduction Induces Large Optic Nerve Head Deformations in Subjects with Normal Tension Glaucoma

Thanadet Chuangsuwanich<sup>1,2</sup>, Tin A. Tun<sup>3,6</sup>, Fabian A. Braeu<sup>1,3</sup>, Xiaofei Wang<sup>4</sup>, Zhi Yun Chin<sup>1,2</sup>, Satish K. Panda<sup>1,2</sup>, Martin Buist<sup>2</sup>, Dan Milea<sup>3,6</sup>, Nicholas Strouthidis<sup>5</sup>, Shamira A. Perera<sup>3,6</sup>, Monisha E. Nongpiur<sup>3,6</sup>, Tin Aung<sup>3,6,7</sup>, Michael JA Girard<sup>1,6,8</sup>

<sup>1</sup>Ophthalmic Engineering & Innovation Laboratory (OEIL), Singapore Eye Research Institute, Singapore National Eye Center, Singapore

<sup>2</sup>Department of Biomedical Engineering, National University of Singapore, Singapore

<sup>3</sup>Singapore Eye Research Institute, Singapore National Eye Centre, Singapore

<sup>4</sup>Beijing Advanced Innovation Center for Biomedical Engineering, Key Laboratory for Biomechanics and Mechanobiology of Ministry of Education, School of Biological Science and Medical Engineering, Beihang University, Beijing, China

<sup>5</sup>NIHR (National Institute of Health Research) Biomedical Sciences Centre, Moorfields Eye Hospital and UCL Institute of Ophthalmology, London, United Kingdom

<sup>6</sup>Duke-NUS Medical School, Singapore

<sup>7</sup>Yong Loo Lin School of Medicine, National University of Singapore

<sup>8</sup>Institute for Molecular and Clinical Ophthalmology, Basel, Switzerland

**Short Title: Adduction Induces Large ONH Deformation in NTG**

## Corresponding Author:

Ophthalmic Engineering & Innovation Laboratory (OEIL), Singapore Eye Research Institute (SERI), The Academia, 20 College Road, Discovery Tower Level 6, Singapore.

E-mail: [mgirard@ophthalmic.engineering](mailto:mgirard@ophthalmic.engineering)

## Introduction

49           The standard biomechanical theory of glaucoma hypothesizes that  
50 biomechanical forces induced by intraocular pressure (IOP) and cerebrospinal fluid  
51 pressure (CSFP) deform the optic nerve head (ONH) tissues, especially at the level  
52 of the lamina cribrosa (LC), yielding retinal ganglion cell (RGC) death.<sup>1</sup> However,  
53 IOP and CSFP are not the only loads that can significantly deform the ONH.  
54 Biomechanical forces exerted by extraocular muscles during eye movements have  
55 been shown to induce significant ONH deformations.<sup>2</sup> Wang et al. have quantified  
56 the effective strain in the LC during eye movements *in vivo* and reported that  
57 adduction could induce as much effective strain (i.e. deformation) to the ONH tissue  
58 as would an IOP elevation to 40 mmHg.<sup>3</sup> This is because the optic nerve can  
59 become ‘taut’ during adduction and exert a significant traction force to the ONH  
60 tissues, as was evidenced through MRI and finite element studies.<sup>4-7</sup> The functional  
61 consequences of such a force are yet unknown.

62           With the high prevalence of normal tension glaucoma (NTG), especially in  
63 some Asian populations<sup>8, 9</sup>, the IOP-centric biomechanical theory of glaucoma is  
64 insufficient to explain the disease etiology. Vascular deficiency in NTG patients has  
65 been proposed as a potential contributing factor,<sup>10</sup> but its evidence is still not  
66 conclusive<sup>11</sup>. From a biomechanical perspective, a few other IOP-independent  
67 factors could contribute to the development of NTG; for instance, a low CSFP<sup>12, 13</sup>,  
68 structural weaknesses of ocular tissues<sup>14, 15</sup>, an increased susceptibility to optic  
69 nerve traction during eye movements<sup>3, 5</sup>, or a combination of the aforementioned  
70 factors. To date, no studies have compared the biomechanical effects of optic nerve  
71 traction in NTG and high-tension glaucoma (HTG) subjects in a relatively large  
72 cohort. With increasing evidence that eye movements could induce significant  
73 deformation in the ONH, both observed *in vivo*<sup>3</sup> and via computational modelling<sup>16</sup>,

74 we believe that such a comparative study could give a valuable insight into the role  
75 of eye movements in glaucoma etiology.

76 The aim of this study was to map *in vivo* deformation and strain of the ONH  
77 tissues in response to changes in gaze positions (abduction and adduction) and to  
78 IOP elevation, in both subjects with HTG and NTG. Similar to our previous works<sup>3, 17,</sup>  
79 <sup>18</sup>, we employed a digital displacement and strain mapping algorithm on spectral  
80 domain optical coherence tomography (OCT) images to quantify *in vivo* ONH strains  
81 in each subject. We hypothesize that NTG and HTG subjects may have different  
82 sensitivities to different biomechanical loads induced by eye movements.

## 83 **Methods**

84 Our goal was to quantitatively map and compare 3D ONH deformations in NTG  
85 and HTG subjects under the following loads – IOP elevation, adduction and  
86 abduction. To this end, we first imaged each subject's ONH in primary gaze using  
87 OCT, and subsequently, under each load. ONH tissue deformations were mapped  
88 using a digital volume correlation (DVC) algorithm applied to pairs of OCT volumes.  
89 Such deformations were then statistically compared across groups (NTG vs HTG),  
90 ONH regions, and ONH tissues. Below is a detailed description of our methodology.

### 91 ***Subjects Recruitment***

92 We recruited 114 subjects with HTG and 114 with NTG from glaucoma clinics  
93 at the Singapore National Eye Centre. We included subjects aged more than 50  
94 years old, of Chinese ethnicity (predominant in Singapore), with a refractive error of  
95  $\pm 3$  diopters, who are currently receiving IOP-lowering medications. We excluded  
96 subjects who underwent prior intraocular/orbital/brain surgeries, subjects with history  
97 of strabismus, ocular trauma, ocular motor palsies, orbital/brain tumors; with clinically  
98 abnormal saccadic or pursuit eye movements; subjects with poor LC visibility in OCT

99 (<50% *en-face* visibility); subjects with known carotid or peripheral vascular disease;  
100 or with any other abnormal ophthalmic and neurological conditions. Glaucoma was  
101 defined as glaucomatous optic neuropathy, characterized as loss of neuroretinal rim  
102 with vertical cup-to-disc ratio >0.7 or focal notching with nerve fiber layer defect  
103 attributable to glaucoma and/or asymmetry of cup-to disc ratio between eyes >0.2,  
104 with repeatable glaucomatous visual field defects (independent of the IOP value) in  
105 at least 1 eye. NTG subjects had low/normal IOP (<21 mmHg) before treatment in  
106 the study eye; HTG subjects had elevated IOP (>=21 mmHg) before treatment in the  
107 study eye. NTG and HTG categorization was established based on IOP values  
108 obtained from Goldmann tonometry.

109 Each subject underwent the following ocular examinations: (1) measurement  
110 of refraction using an autokeratometer (RK-5; Canon, Tokyo, Japan) and (2)  
111 measurement of axial length, central corneal thickness and anterior chamber depth  
112 using a commercial device (Lenstar LS 900; Haag-Streit AG, Switzerland). For each  
113 tested eye we performed a visual field test using a standard achromatic perimetry  
114 with the Humphrey Field Analyser (Carl Zeiss Meditec, Dublin, CA).

115 This study was approved by the SingHealth Centralized Institutional Review  
116 Board and adhered to the tenets of the Declaration of Helsinki. Written informed  
117 consent was obtained from each subject.

### 118 ***OCT Imaging***

119 One eye of each subjects was analyzed. If both eyes had similar diagnosis,  
120 then we selected the study eye at random for each subject; and the ONH was  
121 imaged with spectral-domain OCT (Spectralis; Heidelberg Engineering GmbH,  
122 Heidelberg, Germany). The imaging protocol was similar to that from our previous  
123 work.<sup>3</sup> In brief, we conducted a raster scan of the ONH (covering a rectangular

124 region of  $15^\circ \times 10^\circ$  centered at the ONH), comprising of 97 serial B-scans, with each  
125 B-scan comprising of 384 A-scans (**Figure 1a**). The average distance between B-  
126 scans was  $35.1 \mu\text{m}$  and the axial and lateral B-scan pixel resolution were on  
127 average  $3.87 \mu\text{m}$  and  $11.5 \mu\text{m}$  respectively. All A-scans were averaged 20 times  
128 during acquisition to reduce speckle noise. Each eye was scanned four times under  
129 four different conditions – primary OCT position,  $20^\circ$  adduction,  $20^\circ$  abduction and  
130 acute IOP elevation. Each subject was administered with 1.0% Tropicamide to dilate  
131 the pupils before imaging.

### 132 ***OCT imaging in primary gaze and in Adduction/Abduction*** 133 ***positions***

134 In this study, the primary gaze OCT position referred to the eye position  
135 during a standard OCT scan. Such a position does not exactly correspond to the  
136 primary gaze position as both the pupil and ONH need to be aligned with the OCT  
137 objective, inducing a slight eye rotation to the left in a right eye, and vice versa<sup>3</sup>.  
138 Amplitudes of horizontal gaze positions reported in this study were therefore with  
139 respect to the primary gaze OCT position. Procedures for imaging under different  
140 gaze positions have been described in our previous work<sup>3</sup>. Briefly, we employed a  
141 custom-built 3D printed rotatable chin rest to induce  $20^\circ$  adduction and  $20^\circ$  abduction  
142 and one OCT volume was acquired in each position.

### 143 ***OCT imaging during acute IOP elevation***

144 For each eye in the primary gaze position, we applied a constant force of 0.65  
145 N to the temporal side of the lower eyelid using an ophthalmodynamometer, as per a  
146 well-established protocol.<sup>3, 19</sup> This force raised IOP to about 35 mmHg and was  
147 maintained constant throughout the entire OCT acquisition (approximately 3-5

148 minutes). IOP was then re-assessed with a Tono-Pen (Reichert, Inc.), and the ONH  
149 was imaged with OCT in primary gaze position.

### 150 ***Digital Alignment of OCT volumes***

151 To improve the performance of our deformation mapping protocol, it is first  
152 necessary to remove rigid-body translations and rotations that are present due to  
153 head and/or eye movements of the subjects in between OCT acquisitions. To this  
154 end, each OCT volume under a biomechanical load (adduction, abduction, or  
155 elevated IOP) was digitally aligned with its corresponding primary gaze OCT volume  
156 using a commercial software Amira (version 2020.1, FEI, Hillsboro, Oregon, USA),  
157 as described in our previous publication.<sup>20</sup>

### 158 ***ONH Reconstruction through Automatic Segmentation***

159 For each ONH, we automatically segmented the following tissue groups - the  
160 pre-lamina tissue (PLT, inclusive of retina), the choroid, the sclera and the LC  
161 (**Figure 1a-b**) - using a deep-learning algorithm similar to that designed in our  
162 previous work.<sup>21, 22</sup> This was done, so that we can report deformation and strains for  
163 each tissue group. Bruch's membrane opening (BMO) points were also automatically  
164 extracted with a custom algorithm. Note that BMO points lie within a plane (the BMO  
165 plane), and such a plane can be used as a horizontal reference plane for each ONH.

### 166 ***In Vivo Displacement and Strain Mapping of the ONH***

167 We used a commercial DVC module (*Amira*. (2020.3). Waltham,  
168 Massachusetts: Thermo Fisher Scientific) to map the three-dimensional  
169 deformations of the following OCT volume pairs – **(1)** primary gaze vs acute IOP  
170 elevation, **(2)** primary gaze vs adduction, and **(3)** primary gaze vs abduction – for  
171 each patient. The working principle of this commercial DVC module is similar to our  
172 prior DVC implementation<sup>18</sup>, albeit with an improved speed efficiency. Details of the

173 DVC algorithm used in this study is provided in **Appendix A**. Briefly, each ONH  
174 morphology was sub-divided into ~4000 cubic elements, and ~3,500 nodes (points),  
175 at which locations 3D displacements (vectors) were mapped following a change in  
176 load (i.e., IOP, adduction, or abduction). We then derived the effective strain from the  
177 3D displacements. The effective strain is a convenient local measure of 3D  
178 deformation that takes into account both the compressive and tensile effects. In  
179 other words, the higher the compressive or tensile strain, the higher the effective  
180 strain. Details of the strain derivation is provided in **Appendix B**, and further  
181 validation of the DVC and its effects on strain in **Appendix C**.

### 182 ***Definition of ONH regions***

183 To ensure un-biased comparisons between groups (NTG vs HTG) for 3D  
184 deformations/strains, we first limited our *en-face* field-of-view to a region of 2800 x  
185 2800  $\mu\text{m}^2$  centered on the BMO center for all ONHs. Each ONH was further divided  
186 into eight regions – inferior, superior, nasal, and temporal from either the central  
187 (within the BMO circle), or peripheral (outside the BMO circle) regions (**Figure 1c**). It  
188 should be noted that the central region mainly consists of the PLT and LC, whereas  
189 the peripheral region of the retina, choroid and sclera (**Figure 1d**).

### 190 ***Statistics***

191 Statistical analyses were performed using MATLAB (version 2018a, The  
192 MathWorks, Inc., Natick, Massachusetts, USA). Similar to our previous work,<sup>19</sup>  
193 strains and displacements were defined as continuous variable and the subjects'  
194 diagnoses (HTG and NTG) were defined as categorical variables. We used  
195 independent samples t-test to compare the mean values of effective strain and  
196 displacements between the two diagnostic groups. Furthermore, we used Wilcoxon  
197 Signed Ranked test to investigate the influence of different loads on the median

198 values of effective strain and displacements. To study the variation of displacements  
199 and effective strain between each of the defined ONH regions (**Figure 1c-d**),  
200 displacements and effective strain were defined as continuous variable and each  
201 region was defined as a categorical variable and the mean and median values of the  
202 effective strain were extracted for each of the ONH region. The differences in  
203 regional effective strain values were analyzed using generalized estimating  
204 equations (GEE), performed using *R* (version 4.0.3; R Foundation, Vienna, Austria)  
205 in order to account for inter-region associations. Lastly, to compare the effective  
206 strain across different tissues, we also used GEE with effective strain defined as a  
207 continuous variable and each tissue type as categorical variables. Statistical  
208 significance level for this study was set at 0.05.

## 209 **Results**

### 210 ***Demographics and IOP elevation***

211 A total of 228 Chinese subjects were recruited (consisting of 114 subjects with  
212 HTG and 114 with NTG). We excluded 10 HTG subjects and 8 NTG subjects from  
213 the study due to a low *en-face* LC visibility (<50% of the BMO area) and therefore  
214 104 HTG subjects and 106 NTG subjects were included in the final analysis. Out of  
215 104 HTG subjects, 37 subjects were female. Out of 106 NTG subjects, 49 subjects  
216 were female.

217 There were no significant differences ( $p > 0.05$ , **Table 1**) across both groups in  
218 terms of age [HTG:  $69 \pm 5$ , NTG:  $67 \pm 6$ ], systolic blood pressure [HTG:  $141 \pm 16$   
219 mmHg, NTG:  $140 \pm 20$  mmHg], diastolic blood pressure [HTG:  $75 \pm 9$  mmHg, NTG:  
220  $74 \pm 9$  mmHg], axial length [HTG:  $24.2 \pm 1.0$  mm, NTG:  $24.4 \pm 1.0$  mm], visual field  
221 mean deviation [HTG:  $-7.54 \pm 5.05$  dB, NTG:  $-6.56 \pm 4.91$  dB], pattern standard



222 deviation [HTG:  $7.18 \pm 3.79$  dB, NTG:  $7.22 \pm 3.05$  dB], baseline IOP (on the day of  
223 the experiment) [HTG:  $17.3 \pm 2.9$  mmHg, NTG:  $16.0 \pm 2.5$  mmHg], and IOP during  
224 ophthalmodynamometer indentation [HTG:  $34.5 \pm 7.0$  mmHg, NTG:  $34.8 \pm 6.5$   
225 mmHg].

226 Retinal nerve fiber layer (RNFL) thickness of the NTG subjects were  
227 significantly higher on average as compared to that of the HTG subjects [NTG:  $67.4$   
228  $\pm 36.0$   $\mu\text{m}$ , HTG:  $59.3 \pm 35.5$   $\mu\text{m}$ ,  $p < 0.001$ ].

### 229 ***IOP induces posterior displacements, while adduction induces*** 230 ***anterior displacements in the LC***

231 On average across all subjects, IOP elevation induced posterior  
232 displacements of the LC (with respect to the BMO plane) [ $-5.50 \pm 6.73$   $\mu\text{m}$ ], while  
233 abduction and adduction induced anterior displacements [ $+0.72 \pm 9.85$   $\mu\text{m}$  and  
234  $+1.29 \pm 6.31$   $\mu\text{m}$  respectively] (**Figure 2a**).

### 235 ***Adduction induces transverse shearing of the PLT***

236 Under adduction, we observed a distinct ‘seesaw’ displacement pattern (i.e.,  
237 shearing in the transverse plane) in the PLT with, on average, anterior  
238 displacements in the nasal region [ $+8.17 \pm 9.31$   $\mu\text{m}$ ] and posterior displacements in  
239 the temporal region [ $-5.65 \pm 8.28$   $\mu\text{m}$ ], with significant difference across two regions  
240 ( $p < 0.001$ ) (**Figure 2b-c**). Abduction resulted in an opposite trend of lesser magnitude  
241 (posterior displacement nasally [ $-2.12 \pm 6.53$   $\mu\text{m}$ ] and anterior temporally [ $+2.23 \pm$   
242  $6.51$   $\mu\text{m}$ ]), with significant difference across the two regions ( $p < 0.001$ ). Overall, these  
243 trends were also observed for the choroid and sclera.

### 244 ***IOP and adduction induce equivalently high effective strain in the*** 245 ***LC***

246 We observed that both IOP elevation and adduction induce equivalently high  
247 effective strain in the LC [ $4.46 \pm 2.4\%$  and  $4.42 \pm 2.3\%$ , respectively; no significant  
248 difference,  $p = 0.76$ ]. Abduction induced significantly lower effective strain [ $3.12 \pm$   
249  $1.91\%$ ] than both IOP elevation and adduction ( $p < 0.014$ ; **Figure 3**).

250 ***NTGs are more sensitive to deformations under adduction, while***  
251 ***HTGs under IOP elevation***

252 Under IOP elevation, HTG subjects experienced higher effective strain than  
253 NTG in all tissues, with a statistically significant difference observed in the LC tissue  
254 [HTG LC:  $4.56 \pm 1.74\%$  vs NTG LC:  $4.12 \pm 1.46\%$ ,  $p = 0.047$ ] (**Figure 4a**). Under  
255 Adduction, NTG subjects experienced higher effective strain than HTG subjects in all  
256 tissues (**Figure 4b**), with a statistically significant difference observed in the LC  
257 tissue [NTG LC:  $4.93 \pm 1.88\%$  vs HTG LC:  $4.00 \pm 1.40\%$ ,  $p = 0.041$ ] and in the PLT  
258 [NTG PLT:  $4.56 \pm 1.44\%$  vs HTG PLT:  $3.86 \pm 1.23\%$ ,  $p = 0.002$ ]. Under abduction,  
259 no significant differences in effective strain were observed between NTG and HTG  
260 subjects.

261 ***Regional variations in ONH effective strain***

262 Across all subjects, the central region of the ONH experienced significantly  
263 higher effective strain than the peripheral region under IOP elevation [central region:  
264  $4.68 \pm 1.31\%$  vs peripheral region:  $3.90 \pm 1.13\%$ ,  $p < 0.001$ ] and under adduction  
265 [central region:  $4.53 \pm 1.52\%$  vs peripheral region:  $3.61 \pm 1.12\%$ ,  $p < 0.001$ ] (**Figure**  
266 **5**).

267 Significantly higher effective strain was observed in the peripheral-nasal  
268 region as compared to the peripheral-temporal region under adduction [peripheral-  
269 nasal:  $4.05 \pm 1.50\%$  vs peripheral-temporal:  $3.57 \pm 1.20\%$ ,  $p < 0.001$ ] (**Figure 5**).

270 For abduction, a homogenous distribution of effective strain was observed  
271 with no significant differences across nasal-temporal regions (**Figure 5**).

272

## 273 **Discussion**

274 In this study, we were able to map *in vivo* three-dimensional deformations of  
275 the ONH tissues in subjects with HTG and NTG under the presence of  
276 biomechanical loads, namely, acute IOP elevation, and optic nerve traction in  
277 adduction and abduction. Overall, we found that adduction resulted in large ONH  
278 deformations that were on the same order of magnitude as those induced by an  
279 acute IOP increase to 35 mmHg. In addition, the ONH of HTG subjects was more  
280 mechanically sensitive to IOP compared to whereas that of NTG subjects to  
281 adduction. To the best of our knowledge, this is the first study to quantitatively  
282 compare *in vivo* ONH deformations between NTG and HTG subjects under different  
283 biomechanical loads.

284 We found that adduction (but not abduction) resulted in ONH deformations  
285 and strains that were on the same order of magnitude as those induced by an IOP to  
286 35 mmHg. These findings are consistent with those from our previous studies;<sup>3, 16</sup> we  
287 have simply confirmed this trend in glaucoma eyes. Since adduction stresses the  
288 ONH to a similar level as an acute IOP increase, we could potentially consider  
289 adduction as a clinical stress test to assess the robustness of the ONH *in vivo*. The  
290 advantage being that imaging the eye in adduction is user-friendly and does not  
291 require IOP manipulations that could be of discomfort to the patients. We are  
292 currently investigating the relevance of such a stress test in predicting glaucoma  
293 progression. We also found that adduction generated significantly higher ONH  
294 deformations and strains than abduction; this observation may be explained by the

295 fact that the distance between orbital apex and the ONH is larger following adduction  
296 as compared to abduction, which results in a taut optic nerve and a high optic nerve  
297 traction during adduction.

298 Under IOP elevation, we found that the LC of HTG subjects was subjected to  
299 significantly higher effective strain than the LC of NTG subjects. In short, HTG  
300 subjects were found to be more sensitive to IOP elevation as compared to NTG  
301 subjects, and the difference in sensitivity was most pronounced in the LC tissue.  
302 Since the LC strains are governed by many factors - for instance, the stiffness of the  
303 LC itself<sup>23</sup>, the geometry of the eye<sup>23</sup>, the stiffness of the surrounding sclera<sup>24</sup> and  
304 the complex interactions of the aforementioned parameters - it is difficult to formulate  
305 a biomechanical explanation for the observed differences. Experimental and  
306 computational modelling studies agree on the importance of sclera being the main  
307 load-bearing tissue of the eye<sup>24, 25</sup> and the factors that determine the load-bearing  
308 capacity of the sclera are its shape (thickness and geometry) and its stiffness  
309 modulus. A stiffer peripapillary sclera tissue in general was found to reduce the  
310 magnitude of biomechanical strains within the LC.<sup>26, 27</sup> A thin posterior sclera was  
311 found to deform more than the thick sclera under a given load, resulting in a greater  
312 scleral canal expansion and LC deformation.<sup>28</sup> Indeed, the combinations of other  
313 parameters in the ONH could outweigh the contribution of the sclera to the ONH  
314 structural strength, sometimes resulting in a high IOP-induced LC strain despite the  
315 presence of a stiff sclera. Notwithstanding the complexity of ONH biomechanics, we  
316 still believe that the ONH tissues' stiffnesses and geometries, particularly that of the  
317 sclera, are important to formulate a systematic biomechanical model that explains  
318 the difference in IOP-induced LC strains between NTG and HTG subjects. To the  
319 best of our knowledge, the tissues' properties of NTG eyes have not been studied.

320 Future work which aims to quantify the tissue properties of NTG eyes may allow us  
321 to develop a deeper understanding of the clinically relevant factors that moderate the  
322 influence of IOP elevation in NTG subjects.

323 In this experiment, NTG subjects performing adduction experienced higher  
324 effective strain than HTG subjects across all tissues, with a statistically significant  
325 difference in the PLT and LC. To explain this, we may again consider the hypothesis  
326 that a taut optic nerve acts on the ONH under adduction. It follows then that the  
327 degree of force exerted by a taut optic nerve depends on its stiffness (i.e. a stiffer  
328 optic nerve will transfer more force to the ONH)<sup>4</sup> and its length (i.e. a shorter optic  
329 nerve will have to stretch more under adduction and will exert more force on ONH).  
330 Thus, it is possible that stiffer and/or shorter optic nerves contribute to the greater  
331 sensitivity of NTG eyes to adduction-induced deformation. Unfortunately, both the  
332 stiffness and length of the optic nerve have not been extensively studied and further  
333 studies are warranted.

334 Interestingly, we observed a transverse shearing of the PLT tissue under  
335 adduction, with the ONH tissue in the nasal region displaced anteriorly and the ONH  
336 tissue in the temporal region displaced posteriorly (**Figure 2c**). This phenomenon  
337 was also observed in abduction (in the opposite direction), although the magnitude of  
338 displacement was significantly less than that of adduction. Similar ONH tissue  
339 displacement patterns in the nasal-temporal regions under adduction had been  
340 documented via a geometric characterization of B-scan images by Wang et al.<sup>3</sup> and  
341 Lee et al.<sup>29</sup> Demer et al. had also shown in an MRI study that, under adduction, the  
342 optic nerve becomes more taut on the temporal side, exerting its ‘pulling’ force  
343 mostly on the temporal peripapillary tissue<sup>4, 30</sup> while indirectly causing the nasal  
344 tissue to displace anteriorly. The anterior displacement of the nasal tissue may be

345 explained by the redistribution of cerebrospinal fluid to the nasal side of the ON as  
346 the ON sheath on the temporal side is flattened during adduction – this phenomena  
347 effectively elevates the CSFP on the nasal side of the ON and the elevated CSFP  
348 ‘pushes’ the nasal peripapillary tissue anteriorly.<sup>30</sup> Our study is the first to show a  
349 transverse shearing under adduction in a large number of glaucoma subjects and  
350 our observations seem to further support the notion that the optic nerve is acting  
351 strongly on the ONH during adduction.

352         Despite the observation in this study that adduction is significantly influencing  
353 the ONH biomechanics, especially for the NTG subjects, more investigations are  
354 needed to associate the role of eye movements to the development of glaucoma.  
355 Clearly, susceptibility of an eye to adduction alone is not sufficient to cause  
356 glaucoma; for instance, a person with a convergent squint (i.e., with one or both eyes  
357 in a permanent state of adduction) is not known to be under risk of developing  
358 glaucoma. We suspect that if adduction is going to cause long term damage to the  
359 ONH tissues, it should come from a repetitive movement pattern that occurs in an  
360 eye with prior biotechnical susceptibilities (e.g., shorter and/or stiffer optic nerve) to  
361 the ONH strains induced by adduction. This effect could also be cumulative over  
362 several years. We can allude this phenomenon to a repetitive neurotrauma that  
363 leads to a neurodegenerative disease; for instance, the amyotrophic lateral sclerosis  
364 (ALS) occurring in football players<sup>31, 32</sup> that may be caused by repeated head  
365 traumas throughout the players’ career. A longitudinal study of glaucoma  
366 progression in NTG subjects in relation to the extent of ONH strains under adduction  
367 may help to elucidate the causal relationship between eye movements and  
368 glaucoma disease.

369 In terms of demographics and clinical characteristics, we found no significant  
370 differences between HTG and NTG subjects, except for the average RNFL thickness  
371 (**Table 1**). Even though functional damage or glaucoma severity (as indicated by  
372 visual field indexes) were comparable between the two groups, the degree of  
373 structural damage (as assessed through RNFL thickness) was different. As  
374 glaucoma eyes remodel differently at different stages of damage,<sup>33</sup> this may have  
375 affected our comparisons, and future work that would consider similar structural  
376 damage is warranted.

377 Several limitations in this study warrant further discussion. First, we did not  
378 consider (or measure) CSFP in this study. Several studies suggested that NTG  
379 patients had lower CSFP as compared to HTG<sup>34-36</sup> and a low CSFP has become one  
380 of the main suspects in the pathogenesis of NTG. In an experimental study, a low  
381 CSFP has been shown to increase the translaminal pressure at the LC, leading to a  
382 similar glaucomatous optic neuropathy as observed during a development of  
383 glaucoma with elevated IOP.<sup>37</sup> Unfortunately, a non-invasive measurement of CSFP  
384 *in vivo* is still not feasible and CSFP is usually estimated from other surrogate  
385 measurements, such as an orbital subarachnoid space width<sup>38</sup> or from a regression  
386 model based mainly on values of blood pressures.<sup>39</sup> If we were able to measure and  
387 vary CSFP *in vivo*, we could then investigate the CSFP's influence on the ONH  
388 deformation. We have shown here that the ONH of NTG and HTG subjects deform  
389 differently under adduction and such comparison with respect to changes in CSFP  
390 would be illuminating to the pathogenesis of NTG. In addition, the differences in  
391 CSFP between NTG and HTG may also contribute to the differences in their  
392 biomechanical responses when subjected to IOP elevation as observed in this study.

393           Second, our method of IOP elevation (ophthalmodynamometer) had a  
394 considerable degree of uncertainties. Even though we tried to keep the force applied  
395 at a constant level, the actual IOP raised still depended on the structural properties  
396 of each subject's eye. This resulted in variations in elevated IOP in both groups of  
397 subjects (**Table 1**). To take into account such variations, we then performed an  
398 analysis to normalize the strain according to the actual IOP raised in each subject  
399 (**Appendix D**; using a linear assumption that could be justified according to Midgett  
400 et al.<sup>40</sup>) and found that the average adjusted LC effective strains under IOP elevation  
401 were still significantly higher for HTG subjects as compared to NTG subjects (HTG:  
402  $6.1\pm 3.2\%$ , NTG:  $4.6\pm 2.3\%$ ,  $p = 0.006$ ).

403           Third, our study was limited to subjects of Chinese ethnicity that were more  
404 than 50 years old. Since age is a well-known factor affecting the biomechanical  
405 properties of the eyes<sup>33, 41, 42</sup> and ethnicity is also another important factor that could  
406 affect glaucoma pathogenesis<sup>43</sup>, further studies should investigate if the reported  
407 differences in biomechanical responses are also present in other demographics.

408           Fourth, the OCT resolution and signal quality of the posterior portion of the  
409 eye (beyond the LC) were poor. Therefore, we were not able to investigate the local  
410 strains of the optic nerve in situ, as well as its sheath insertion into the sclera. We  
411 suspect that the local strains at the site will be large, and this could contribute to  
412 focal defects observed in NTG patients under adduction. In addition, there were  
413 differences in terms of scan resolutions across each dimension (i.e., 11.3 micron for  
414 the lateral resolution and 3.87 micron for the axial direction). One main implication of  
415 the differences in resolution was that the magnitude of displacement error in each  
416 direction would be different. For instance, our displacement measurements were  
417 approximately 3 times more accurate in the axial direction as compared to the lateral



418 direction. Since our effective strain was an ‘average’ measure across all dimensions,  
419 its accuracy would largely be limited by the dimension which had the worst  
420 resolution. For instance, an average displacement error (3 micron) in the lateral  
421 direction would result in approximately 0.6% error in effective strain, whereas an  
422 average displacement error (1 micron) in the axial direction would result in  
423 approximately 0.2% error in effective strain.

424 Fifth, the duration of IOP elevation in our study was short (each patient was  
425 subjected to the ophthalmodynamometer procedure for no longer than 5 minutes).  
426 This time duration may not be enough to evoke a steady-state deformation response  
427 from the tissue. It is likely that we imaged the ONH while it was still in the process of  
428 responding to the applied load. However, from our data, we can still clearly observe  
429 the influence of IOP elevation on the ONH via a distinct posterior deformation  
430 observed in the tissues. Over a long period of time, there may be structural changes  
431 in the ONH that may mitigate against such marked deformations. This may explain  
432 the different rates of progression observed in glaucoma patients early on and later  
433 on in their disease.

434 Sixth, the displacement and effective strain errors from our DVC method were  
435 non-zero. From our validation study, we found that the errors were acceptable when  
436 we conducted deformation tracking on repeated primary gaze scans of healthy  
437 subjects, with displacement errors of less than 30% of the voxel resolution and the  
438 effective strain error of less than 1.2% (**Appendix C**). The errors observed here  
439 could arise from various sources such as OCT registration errors (intrinsic to the  
440 OCT machine), rotation of subjects’ head during OCT acquisition, OCT speckle  
441 noise and IOP fluctuations from ocular pulsations<sup>44</sup>, all of which were difficult to  
442 control. Even though our reported baseline strains error of 1.2% was close to the

443 magnitude of differences in average strains between the two groups, we arrived at  
444 our main conclusions (i.e., significant differences in strains between HTG and NTG),  
445 using a t-test with an appropriate p-value, as opposed to directly comparing the  
446 average value of strains. Thus, our main conclusions were valid within the  
447 assumptions of t-test (i.e., normal distribution of both population, random sampling of  
448 the population etc.).

449 In conclusion, we measured the *in vivo* deformation of ONH tissue in 114  
450 subjects with HTG and 114 with NTG in response to IOP elevation and horizontal  
451 eye movements. We found that **(1)** adduction induced effective strain that was  
452 comparable to that induced by IOP, **(2)** NTG subjects experienced significantly  
453 higher strains due to adduction compared to HTG subjects and **(3)** HTG subjects  
454 (specifically at the LC) experienced significantly higher strain due to IOP elevation  
455 compared to NTG subjects. Our results suggest that NTG and HTG subjects have  
456 distinct responses to IOP elevation and adduction, supporting the hypothesis that  
457 these two have different etiologies of glaucoma damage.

458

459

460

461

462

463

464

465

466

467

468

469

470

471

472

473

474

475

476

477

478

## 479 **Acknowledgement**

### 480 **Financial Support:**

481 This work was supported by (1) the Singapore Ministry of Education, Academic  
482 Research Funds, Tier 2 (R-397-000-280-112; R-397-000-308-112) (2) Singapore  
483 Ministry of Education, Academic Research Funds, Tier 1 (R-397-000-294-114) (3)  
484 the National Medical Research Council (Grant NMRC/STAR/0023/2014) and (4)  
485 National Natural Science Foundation of China (12002025).

486

### 487 **Financial Disclosures:**

488 No financial disclosures.

489

### 490 **Other acknowledgements:**

491 None.

492

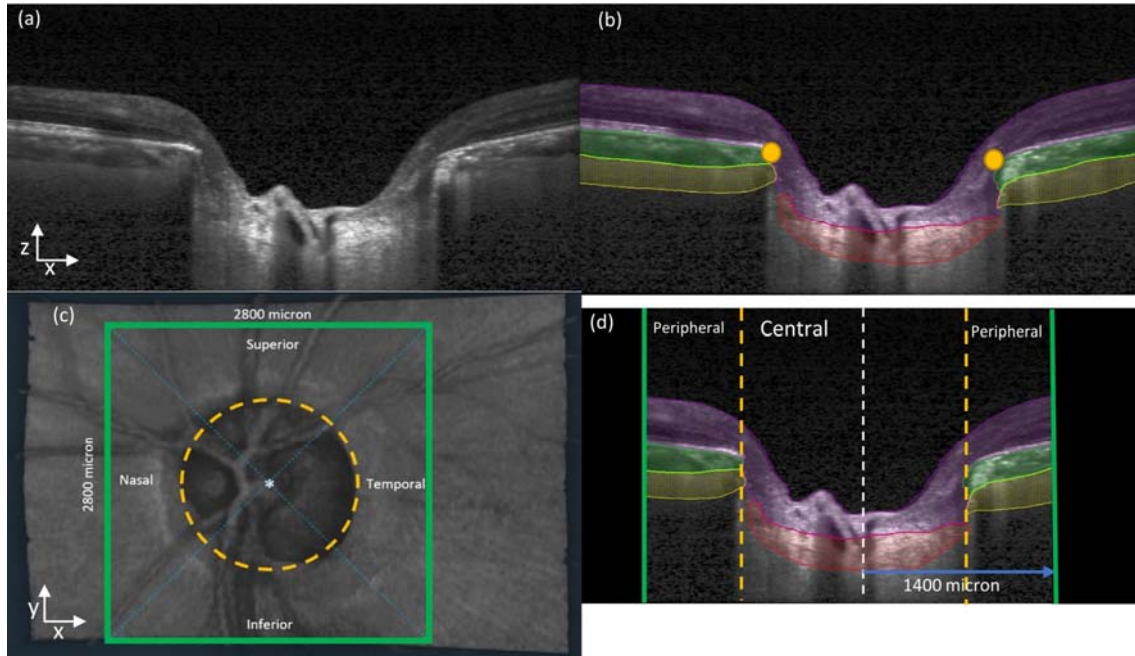
493  
494  
495  
496  
497  
498  
499  
500  
501  
502  
503  
504  
505  
506

Characteristic	Mean $\pm$ standard deviation or n (%)		p-value
	HTG	NTG	HTG – NTG
Age (year)	69 $\pm$ 5	67 $\pm$ 6	0.10
Sex, female (%)	32%	45%	-
Systolic blood pressure (mmHg)	141 $\pm$ 16	140 $\pm$ 20	0.91
Diastolic blood pressure (mmHg)	75 $\pm$ 9	74 $\pm$ 9	0.88
Axial Length (mm)	24.2 $\pm$ 1.0	24.4 $\pm$ 1.0	0.13
Visual field, MD (dB)	-7.54 $\pm$ 5.05	-6.56 $\pm$ 4.91	0.32
Pattern standard deviation (dB)	7.18 $\pm$ 3.79	7.22 $\pm$ 3.05	0.46
Average RNFL thickness ( $\mu$ m)	59.3 $\pm$ 35.5	67.4 $\pm$ 36.0	<0.001
Baseline IOP (mmHg) <sup>□</sup>	17.3 $\pm$ 2.9	16.0 $\pm$ 2.5	0.14
IOP (mmHg) with indentation <sup>□</sup>	34.5 $\pm$ 7.0	34.8 $\pm$ 6.5	0.60

507

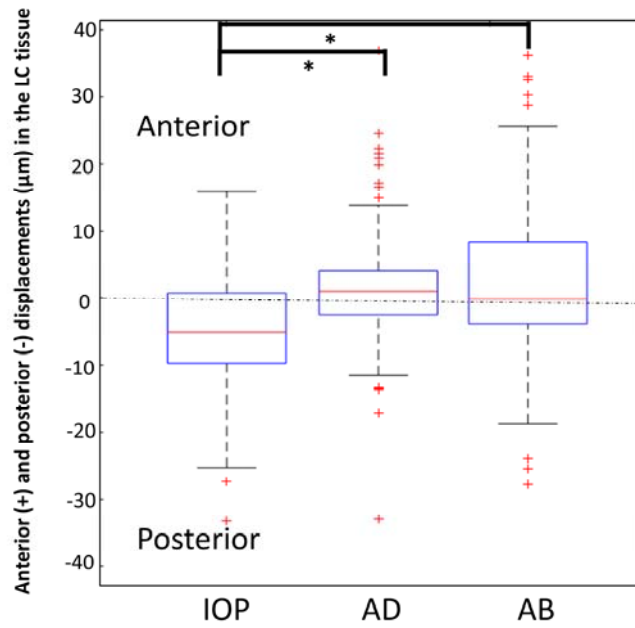
508 **Table 1:** Demographics and clinical characteristics of included study subjects.

509 □ IOP values indicated here are measured at the point of the experiment (after glaucoma  
510 diagnosis and IOP-lowering treatments for both groups)  
511

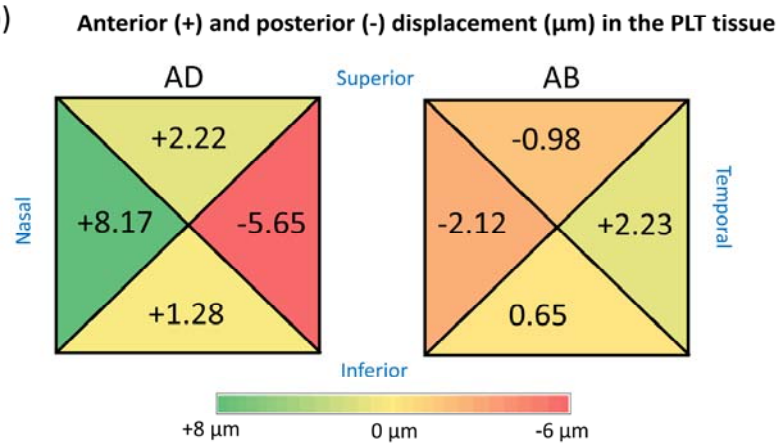


512 **Figure 1(a)** A single B-scan obtained from the OCT machine without any image  
513 enhancement **(b)** Automatic segmentation of the B-scan in (a). Four tissues were  
514 segmented – Pre-Lamina tissue (blue), Choroid (green), Sclera (yellow) and LC (red) In  
515 addition, BMOs (orange dots) were automatically marked for each B-scan **(c)** Anterior-  
516 surface view (X-Y plane) of the ONH. The ONH center (white star) was identified from the  
517 best-fit circle to the BMOs (orange-dotted line). Green square defines our region of interest  
518 to be cropped from the OCT volume with 2800 $\mu$ m length on each side. Diagonal blue lines  
519 define Superior-Inferior-Nasal-Temporal regions of the ONH. **(d)** A B-scan view (X-Z plane)  
520 after we apply cropping to the OCT volumes. Black region was not considered for our  
521 deformation tracking. The length from central line (white-dotted line) to the cropping border  
522 (green line) is 1400  $\mu$ m. The area inside the BMO (orange-dotted line) is defined as central  
523 region while the area outside the BMO is defined as peripheral region.  
524  
525

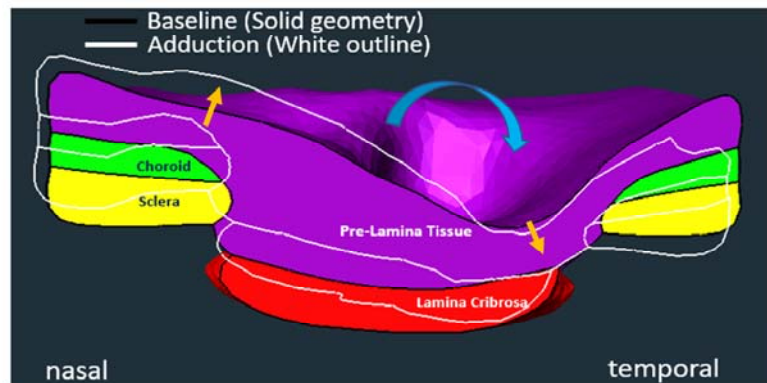
(a)



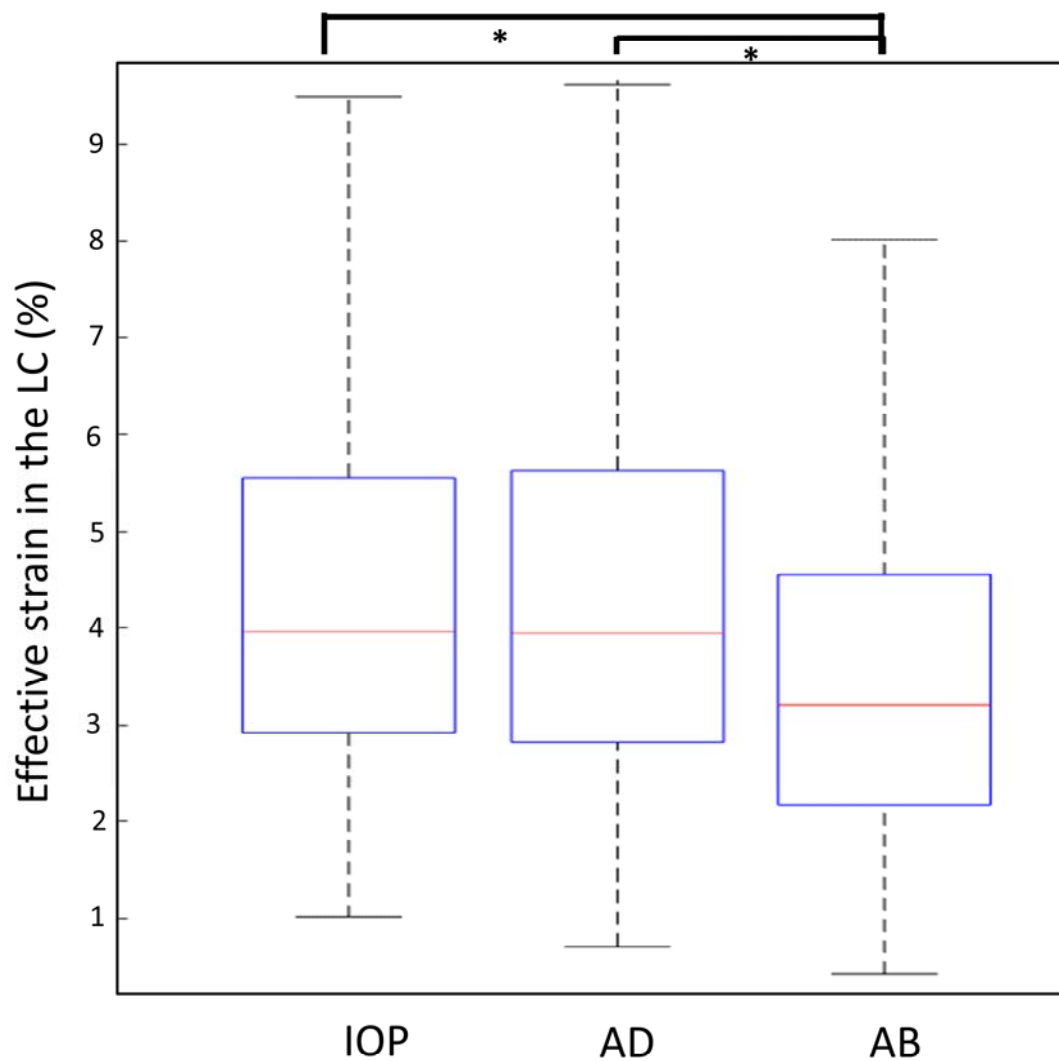
(b)



(c)

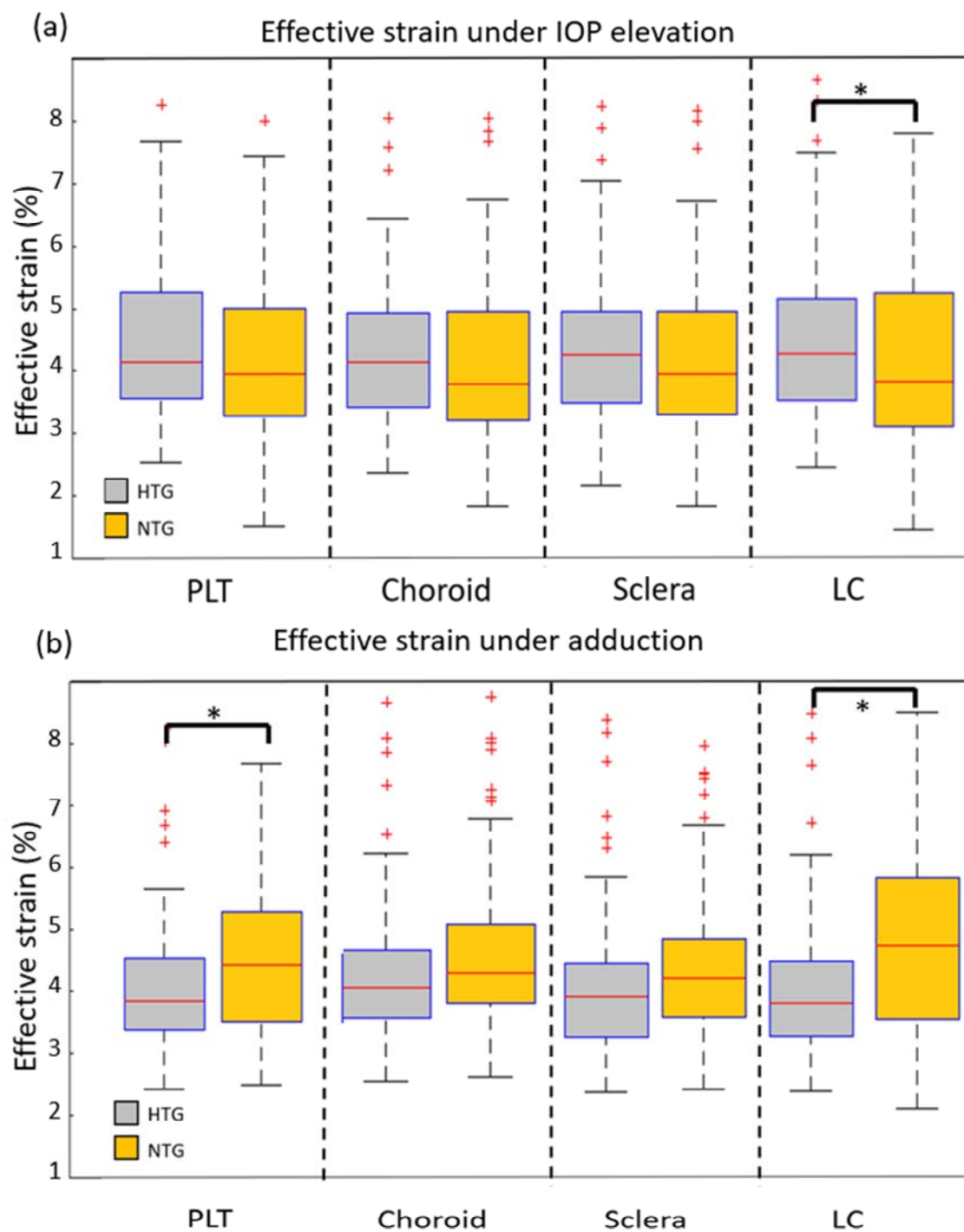


527 **Figure 2(a)** A box plot showing anterior-posterior displacement in  $\mu\text{m}$  in the LC tissue with  
528 respect to each load. (\* indicates significant difference at  $p < 0.05$ ) **(b)** A colored-coded plot of  
529 regional variations in anterior-posterior displacement (in  $\mu\text{m}$ ) in PLT with respect to eye  
530 positions. **(c)** An example of tissue displacement under Adduction obtained from one  
531 subject. Yellow arrows indicate general movement of tissues in nasal and temporal region.  
532 Blue arrow indicates globe rotation direction under adduction. AD: adduction, AB: abduction.



533  
534  
535  
536  
537

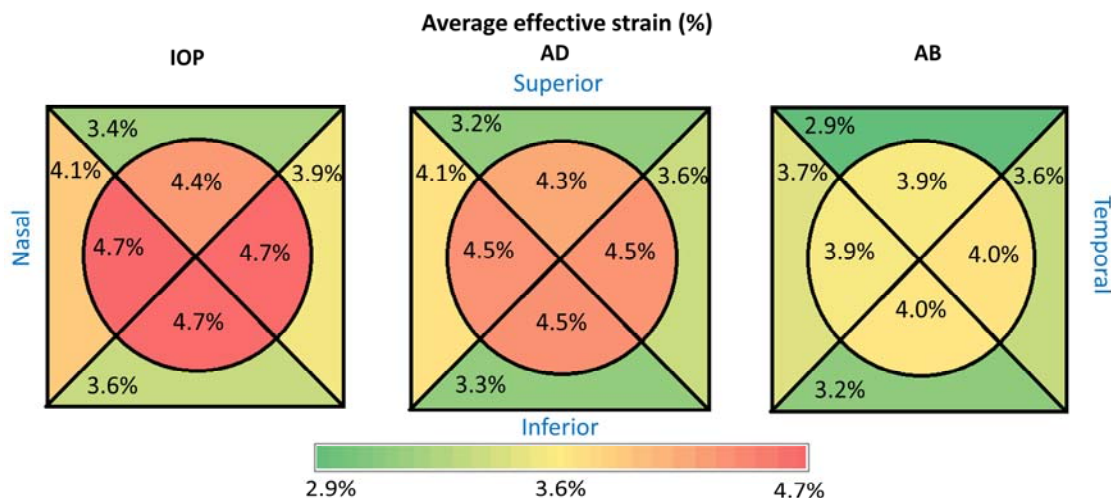
**Figure 3** A box plot showing average effective strain in the LC tissue (%) with respect to each load (\* indicates significant difference at  $p < 0.05$ ). AD: adduction, AB: abduction.



538  
539  
540  
541  
542  
543

**Figure 4(a)** A bar chart showing average effective strain in each tissue (under IOP elevation) for each diagnostic group. **(b)** A bar chart showing average effective strain in each tissue (under adduction) for each diagnostic group (\* indicates significant difference at  $p < 0.05$ ).





544  
545  
546  
547  
548  
549  
550

**Figure 5** A colored-coded plot of regional variations in average effective strain with respect to each load.

## 551 References

552  
553  
554  
555  
556  
557  
558  
559  
560  
561  
562  
563  
564  
565  
566  
567  
568  
569  
570  
571  
572  
573  
574  
575  
576

1. Burgoyne CF, Downs JC, Bellezza AJ, et al. The optic nerve head as a biomechanical structure: a new paradigm for understanding the role of IOP-related stress and strain in the pathophysiology of glaucomatous optic nerve head damage. *Progress in retinal and eye research* 2005;24(1):39-73.
2. Greene PR. Mechanical considerations in myopia: relative effects of accommodation, convergence, intraocular pressure, and the extraocular muscles. *American journal of optometry and physiological optics* 1980;57(12):902-14.
3. Wang X, Beotra MR, Tun TA, et al. In vivo 3-dimensional strain mapping confirms large optic nerve head deformations following horizontal eye movements. *Investigative ophthalmology & visual science* 2016;57(13):5825-33.
4. Demer JL. Optic nerve sheath as a novel mechanical load on the globe in ocular duction. *Investigative Ophthalmology & Visual Science* 2016;57(4):1826-38.
5. Demer JL, Clark RA, Suh SY, et al. Magnetic resonance imaging of optic nerve traction during adduction in primary open-angle glaucoma with normal intraocular pressure. *Investigative ophthalmology & visual science* 2017;58(10):4114-25.
6. Wang X, Rumpel H, Baskaran M, et al. Optic nerve tortuosity and globe proptosis in normal and glaucoma subjects. *Journal of glaucoma* 2019;28(8):691-6.
7. Demer JL, Clark RA, Suh SY, et al. Optic nerve traction during adduction in open angle glaucoma with normal versus elevated intraocular pressure. *Current eye research* 2020;45(2):199-210.
8. Kim C-s, Seong GJ, Lee N-h, et al. Prevalence of primary open-angle glaucoma in central South Korea: the Namil study. *Ophthalmology* 2011;118(6):1024-30.
9. Iwase A, Suzuki Y, Araie M, et al. The prevalence of primary open-angle glaucoma in Japanese: the Tajimi Study. *Ophthalmology* 2004;111(9):1641-8.

- 577 10. Yamamoto T, Kitazawa Y. Vascular pathogenesis of normal-tension glaucoma: a  
578 possible pathogenetic factor, other than intraocular pressure, of glaucomatous optic  
579 neuropathy. *Progress in retinal and eye research* 1998;17(1):127-43.
- 580 11. Mroczkowska S, Benavente-Perez A, Negi A, et al. Primary open-angle glaucoma vs  
581 normal-tension glaucoma: the vascular perspective. *JAMA ophthalmology* 2013;131(1):36-  
582 43.
- 583 12. Lee SH, Kwak SW, Kang EM, et al. Estimated trans-lamina cribrosa pressure  
584 differences in low-teen and high-teen intraocular pressure normal tension glaucoma: the  
585 Korean National Health and Nutrition Examination Survey. *PloS one* 2016;11(2):e0148412.
- 586 13. Chen BH, Drucker MD, Louis KM, Richards DW. Progression of normal-tension  
587 glaucoma after ventriculoperitoneal shunt to decrease cerebrospinal fluid pressure. *Journal*  
588 *of glaucoma* 2016;25(1):e50-e2.
- 589 14. Park JH, Jun RM, Choi K-R. Significance of corneal biomechanical properties in  
590 patients with progressive normal-tension glaucoma. *British Journal of Ophthalmology*  
591 2015;99(6):746-51.
- 592 15. Kim YC, Koo YH, Jung KI, Park CK. Impact of posterior sclera on glaucoma progression  
593 in treated myopic normal-tension glaucoma using reconstructed optical coherence  
594 tomographic images. *Investigative ophthalmology & visual science* 2019;60(6):2198-207.
- 595 16. Wang X, Rumpel H, Lim WEH, et al. Finite element analysis predicts large optic nerve  
596 head strains during horizontal eye movements. *Investigative ophthalmology & visual science*  
597 2016;57(6):2452-62.
- 598 17. Girard MJ, Beotra MR, Chin KS, et al. In vivo 3-dimensional strain mapping of the  
599 optic nerve head following intraocular pressure lowering by trabeculectomy.  
600 *Ophthalmology* 2016;123(6):1190-200.
- 601 18. Girard MJ, Strouthidis NG, Desjardins A, et al. In vivo optic nerve head biomechanics:  
602 performance testing of a three-dimensional tracking algorithm. *Journal of The Royal Society*  
603 *Interface* 2013;10(87):20130459.
- 604 19. Beotra MR, Wang X, Tun TA, et al. In vivo three-dimensional lamina cribrosa strains  
605 in healthy, ocular hypertensive, and glaucoma eyes following acute intraocular pressure  
606 elevation. *Investigative ophthalmology & visual science* 2018;59(1):260-72.
- 607 20. Maes F, Collignon A, Vandermeulen D, et al. Multimodality image registration by  
608 maximization of mutual information. *IEEE transactions on Medical Imaging* 1997;16(2):187-  
609 98.
- 610 21. Devalla SK, Renukanand PK, Sreedhar BK, et al. DRUNET: a dilated-residual U-Net  
611 deep learning network to segment optic nerve head tissues in optical coherence  
612 tomography images. *Biomedical optics express* 2018;9(7):3244-65.
- 613 22. Panda SK, Cheong H, Tun TA, et al. Describing the Structural Phenotype of the  
614 Glaucomatous Optic Nerve Head Using Artificial Intelligence. *American Journal of*  
615 *Ophthalmology* 2021.
- 616 23. Sigal IA. Interactions between geometry and mechanical properties on the optic  
617 nerve head. *Investigative ophthalmology & visual science* 2009;50(6):2785-95.
- 618 24. Sigal IA, Flanagan JG, Ethier CR. Factors influencing optic nerve head biomechanics.  
619 *Investigative ophthalmology & visual science* 2005;46(11):4189-99.
- 620 25. Downs JC, Roberts MD, Burgoyne CF. The mechanical environment of the optic nerve  
621 head in glaucoma. *Optometry and vision science: official publication of the American*  
622 *Academy of Optometry* 2008;85(6):425.

- 623 26. Coudrillier B, Campbell IC, Read AT, et al. Effects of peripapillary scleral stiffening on  
624 the deformation of the lamina cribrosa. *Investigative ophthalmology & visual science*  
625 2016;57(6):2666-77.
- 626 27. Eilaghi A, Flanagan JG, Simmons CA, Ethier CR. Effects of scleral stiffness properties  
627 on optic nerve head biomechanics. *Annals of biomedical engineering* 2010;38(4):1586-92.
- 628 28. Jia X, Yu J, Liao S-H, Duan X-C. Biomechanics of the sclera and effects on intraocular  
629 pressure. *International journal of ophthalmology* 2016;9(12):1824.
- 630 29. Lee WJ, Kim YJ, Kim JH, et al. Changes in the optic nerve head induced by horizontal  
631 eye movements. *PloS one* 2018;13(9):e0204069.
- 632 30. Chang MY, Shin A, Park J, et al. Deformation of optic nerve head and peripapillary  
633 tissues by horizontal duction. *American journal of ophthalmology* 2017;174:85-94.
- 634 31. Abel EL. Football increases the risk for Lou Gehrig's disease, amyotrophic lateral  
635 sclerosis. *Perceptual and motor skills* 2007;104(3\_suppl):1251-4.
- 636 32. Chio A, Benzi G, Dossena M, et al. Severely increased risk of amyotrophic lateral  
637 sclerosis among Italian professional football players. *Brain* 2005;128(3):472-6.
- 638 33. Downs JC. Optic nerve head biomechanics in aging and disease. *Experimental eye*  
639 *research* 2015;133:19-29.
- 640 34. Wang N, Xie X, Yang D, et al. Orbital cerebrospinal fluid space in glaucoma: the  
641 Beijing intracranial and intraocular pressure (iCOP) study. *Ophthalmology*  
642 2012;119(10):2065-73. e1.
- 643 35. Jonas JB, Yang D, Wang N. Intracranial pressure and glaucoma. *Journal of glaucoma*  
644 2013;22:S13-S4.
- 645 36. Cha S, Jeong S, Oh H, et al. Estimated cerebrospinal fluid pressure in normal tension  
646 glaucoma versus high tension glaucoma in Korean population based study. *Investigative*  
647 *Ophthalmology & Visual Science* 2015;56(7):5006-.
- 648 37. Yablonski M, Ritch R, Pokorny K. Effect of decreased intracranial-pressure on optic  
649 disk. *Investigative Ophthalmology & Visual Science: LIPPINCOTT-RAVEN PUBL 227 EAST*  
650 *WASHINGTON SQ, PHILADELPHIA, PA 19106, 1979.*
- 651 38. Xie X, Chen W, Li Z, et al. Noninvasive evaluation of cerebrospinal fluid pressure in  
652 ocular hypertension: a preliminary study. *Acta ophthalmologica* 2018;96(5):e570-e6.
- 653 39. Fleischman D, Bicket AK, Stinnett SS, et al. Analysis of cerebrospinal fluid pressure  
654 estimation using formulae derived from clinical data. *Investigative Ophthalmology & Visual*  
655 *Science* 2016;57(13):5625-30.
- 656 40. Midgett DE, Quigley HA, Nguyen TD. In vivo characterization of the deformation of  
657 the human optic nerve head using optical coherence tomography and digital volume  
658 correlation. *Acta biomaterialia* 2019;96:385-99.
- 659 41. Kotecha A. What biomechanical properties of the cornea are relevant for the  
660 clinician? *Survey of ophthalmology* 2007;52(6):S109-S14.
- 661 42. Strouthidis NG, Girard MJ. Altering the way the optic nerve head responds to  
662 intraocular pressure—a potential approach to glaucoma therapy. *Current opinion in*  
663 *pharmacology* 2013;13(1):83-9.
- 664 43. Sample PA, Girkin CA, Zangwill LM, et al. The african descent and glaucoma  
665 evaluation study (ADAGES): Design and baseline data. *Archives of ophthalmology*  
666 2009;127(9):1136-45.
- 667 44. Pitchon E, Leonardi M, Renaud P, et al. First in vivo human measure of the  
668 intraocular pressure fluctuation and ocular pulsation by a wireless soft contact lens sensor.  
669 *Investigative Ophthalmology & Visual Science* 2008;49(13):687-.

